



Neutral lithium spectral line 460.28 nm with forbidden component for low temperature plasma diagnostics of laser-induced plasma[☆]



M. Cvejić^a, E. Stambulchik^b, M.R. Gavrilović^{a,c}, S. Jovičević^a, N. Konjević^{d,*}

^a Institute of Physics, University of Belgrade, P.O. Box 68, 11081 Belgrade, Serbia

^b Faculty of Physics, Weizmann Institute of Science, Rehovot 7610001, Israel

^c Faculty of Electrical Engineering, University of Belgrade, 11120 Belgrade, Serbia

^d Faculty of Physics, University of Belgrade, P.O. Box 368, 11001 Belgrade, Serbia

ARTICLE INFO

Article history:

Received 9 May 2014

Accepted 6 June 2014

Keywords:

Laser induced plasma
Spectroscopic plasma diagnostic
Stark broadening
Line with forbidden component
Lithium

ABSTRACT

We present the results of theoretical and experimental line shape study of the Li I 460.28 nm line with a forbidden component in a low temperature laser-induced plasma. For this purpose a computer simulation method is used to calculate the overall line profile in the electron number density range of $(0.5\text{--}11.0) \times 10^{16} \text{ cm}^{-3}$ and the electron temperature 5800 K. The same computer simulation method is used to evaluate asymmetric profiles of the isolated Li I 497.17 nm line in the same electron density range and for several electron temperatures between 3500 K and 10300 K. The results for the Li I isolated line are used together with two other theoretical calculations for independent electron density measurements in laser induced plasma. The electron temperatures in the range of 4000–7000 K were determined from relative Li I line intensities using Boltzmann plot technique. The comparison between calculated profiles and experimental data for the Li I 460.28 nm line with a forbidden component indicates that theoretical results can be used for electron density diagnostics in the aforementioned density range with an accuracy of $\pm 10\text{--}15\%$. To facilitate the application of theoretical line profiles simple expressions are supplied.

© 2014 Elsevier B.V. All rights reserved.

1. Introduction

Spatial and temporal distributions of plasma electron number density (N_e) are among the most important plasma parameters required for testing of plasma modeling. For the plasma N_e diagnostics, spectral line shapes in conjunction with theoretical calculations are most frequently used. For this purpose, a spectral line profile is usually recorded using optical emission spectroscopy technique, but absorption or induced fluorescence may be used as well. For N_e determination the experimental line widths or the whole line profiles are compared with corresponding results of well tested theoretical calculations. The most sensitive line shapes for N_e plasma diagnostics belong to hydrogen atom or hydrogen-like ion with line shapes governed by the linear Stark effect. However, hydrogen is not always present in plasma and sometimes is avoided; in these cases isolated lines of non-hydrogenic species are often used for plasma diagnostics. Since the shapes of these lines are governed by the quadratic Stark effect, they are narrower and overlap less with neighboring lines. This in some cases is a great advantage in comparison with broad hydrogen lines. Furthermore, non-hydrogenic lines are available almost in all regions of emission spectra which is important for numerous applications. Unfortunately, large volume of

theoretical Stark broadening data for non-hydrogenic lines is still missing, while not all available data have been thoroughly tested. Thus, for the application of a spectral line not studied before, laborious calculations and their testing are required. This is in particular a case for lines of heavier elements frequently required for various laser-induced breakdown spectroscopy (LIBS) applications.

The situation is considerably relaxed if results of theoretical calculations are available. In this case it is important that theory was used for calculation of tested spectral line profile parameters belonging to other elements or other transitions of the same element. Another difficulty frequently met with non-hydrogenic lines is that they are in some cases so spectrally narrow that it limits correct determination of line shape with typical spectroscopic equipment used in laboratory for LIBS experiments.

The lack of Stark broadening data for neutral and singly charged ion lines explains a recent increase in experimental studies and testing of theoretical predictions of line shapes. An overview of earlier publications dealing with Stark broadening studies using laser induced plasma (LIP) as a plasma source is reported in [1]. Since then, several new publications have appeared: Al II lines [2], Zn I 636.2 nm line [3] and indium and zinc neutral lines [4]. In Refs. [5,6] the authors supplemented previously published data on Fe II and Ni II. A large number of Cu I and Cu II lines was studied in [7] while difficulties experienced with Cu I resonance lines and Stark broadening parameters were addressed in [8].

Due to its several advantages, LIP has been used as a plasma source for so many new line shape studies. The most important qualities of a LIP as a light source are: possibility to obtain line emission for a large number of

[☆] This paper is dedicated to Nicoló Omenetto, on the occasion of his 75th birthday, in recognition of his outstanding contributions to the field of laser spectrochemistry and as an editor of Spectrochimica Acta Part B.

* Corresponding author.

E-mail address: nikruz@ff.bg.ac.rs (N. Konjević).

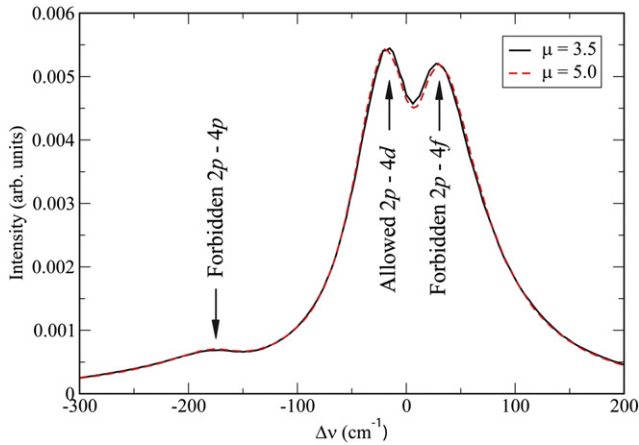


Fig. 1. Effect of the reduced ion mass μ on the Li I 460.28-nm shape. $T = 0.5$ eV ($T = 5800$ K) and $N_e = 10^{17}$ cm $^{-3}$ were assumed. The line shapes are normalized to a unity area. Zero corresponds to a position of unperturbed 2p–4d transition.

elements and their ions in a large range of plasma parameters by simple replacement of the target material, by change of the plasma observation time, by replacement of a surrounding gas, and by change of the laser wavelength and power input to the target surface. These are the main advantages of LIP over other types of gas discharges used for line shape measurements [9]. Certain disadvantages also exist, and the most important one is plasma inhomogeneity, which is changing temporally and spatially during the LIP generation and decay. For proper application of

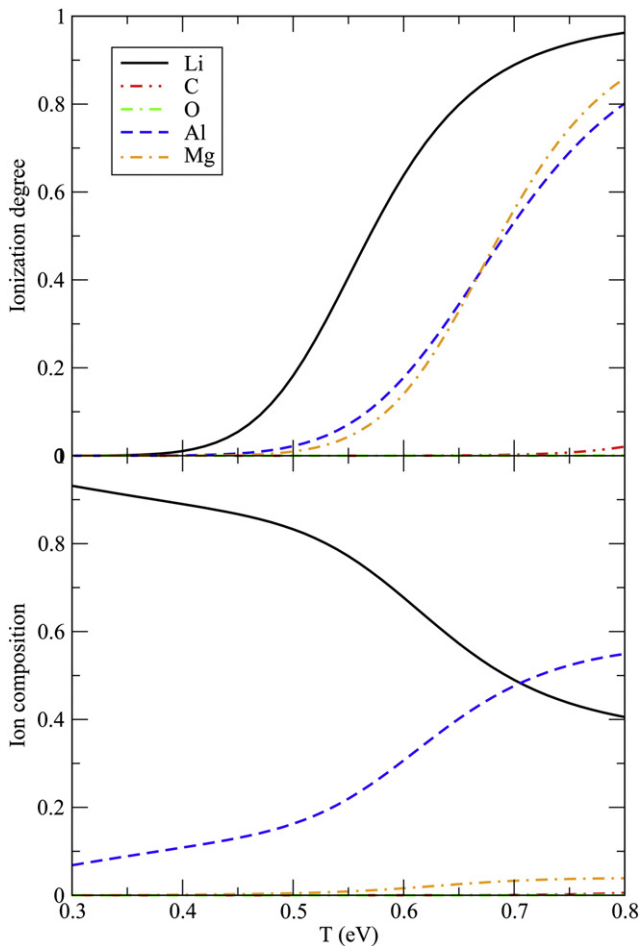


Fig. 2. Ionization degree and ionic plasma composition of a mixture of Al_2O_3 , Li_2CO_3 , and MgCO_3 , in a 9:4:1 proportion at $N_e = 10^{17}$ cm $^{-3}$ and assuming Saha equilibrium.

LIP for line shape recording one has to take care of numerous precautions, which will be discussed and performed in the experimental part of this study.

We present in this work results of an experimental and theoretical line shape study of a spectral line with forbidden component. The width and shape of the overall line profile, depending on the plasma density (N_e) and, to a smaller extent, on the electron temperature (T_e), are somewhere in between non-hydrogenic and hydrogenic profiles. As an intermediate case, these lines with one or more forbidden components (transitions with $\Delta l \neq \pm 1$, where l is angular momentum quantum number) occur as a result of the breakdown of the parity selection rules induced by ambient DC or plasma electric microfield. This effect should not be confused with the forbiddenness associated to magnetic dipole, electric quadrupole or other higher multipole transitions. When plasma broadening of allowed line becomes comparable with energy levels separation between allowed transition and nearest dipole allowed perturbing level or levels, wave functions becomes mixed. In this case normally forbidden line starts to appear close to the allowed one. With an increase of electric field (i.e., an increase of the charged particles density), the mixing of the wave functions becomes stronger, the difference between the allowed and forbidden components becomes meaningful; and one is approaching hydrogen-like emitter approximation with linear Stark effect responsible for the line shape formation. Thus, the overall shape of these lines is sensitive to the charged particle density and, therefore, can be used for the N_e plasma diagnostics. Furthermore, the comparison of an overall experimental profile of a line with forbidden components with results of theoretical calculations may be used as a sensitive test of the Stark broadening theory. The best studied examples are several visible neutral He I lines with forbidden components, see e.g. [10,11]. For recent studies and reviews of relevant literature for two most frequently used He I 447.1 nm and 499.22 nm lines see [12–14] and references therein.

Unfortunately, in a number of plasma sources helium is not present. In some cases like LIP in front of a solid target the diagnostics with helium lines may infer erroneous conclusions due to a poor mixing of the ablated material with the surrounding gas [15]. Furthermore, in low-temperature plasma, He lines are not excited or they are insufficiently intense for reliable N_e diagnostics. Thus, one requires more suitable lines with forbidden components belonging to higher-Z elements that originate from the target material.

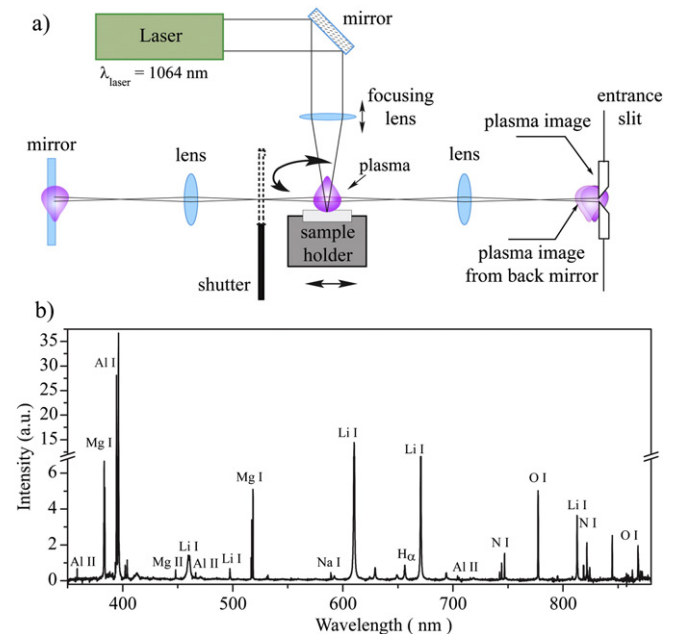


Fig. 3. a) Schematic presentation of the experimental setup. b) Typical overall spectra spatially and temporally integrated, recorded with Mechelle ME5000, Andor Technology.

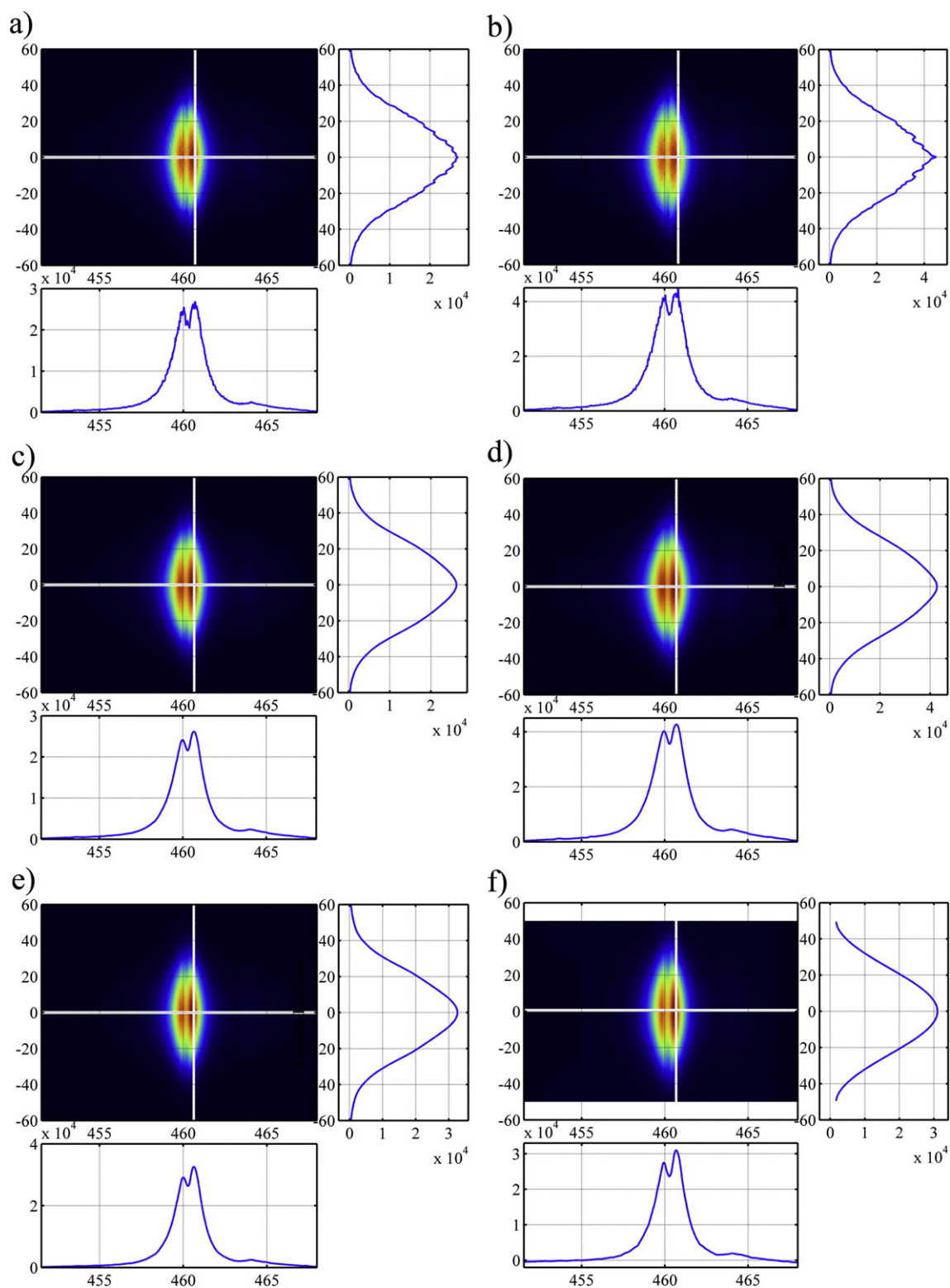


Fig. 4. The steps of experimental data processing for the Li 460.28 nm line recorded at $z = 1.5$ mm from the target surface and recorded with delay time of $3 \mu\text{s}$: a) data matrix recorded without back mirror (WOM) after corrections for apparatus function, wavelength correction, crop and symmetrization; b) data matrix recorded with back mirror (WM) after corrections for apparatus function, wavelength correction, crop and symmetrization; c) WOM after smoothing; d) WM after smoothing; e) data matrix after self-absorption (SA) correction and f) data matrix after Abel inversion.

After helium, the next element in the periodic table is lithium, the lightest metal with a simple atomic structure. This element is used for various applications and found in a number of target materials suitable for LIBS analysis [16–20]. Non-hydrogenic Li I spectral lines have already been the subject of several experimental studies

but only few Stark widths and shifts of Li I lines were reported together with plasma N_e and T_e required for theory testing, see e.g. [9,21].

Among the Li I lines with forbidden components, the most studied is the Li I 460.28 nm line. The allowed line at 460.28 nm originates from

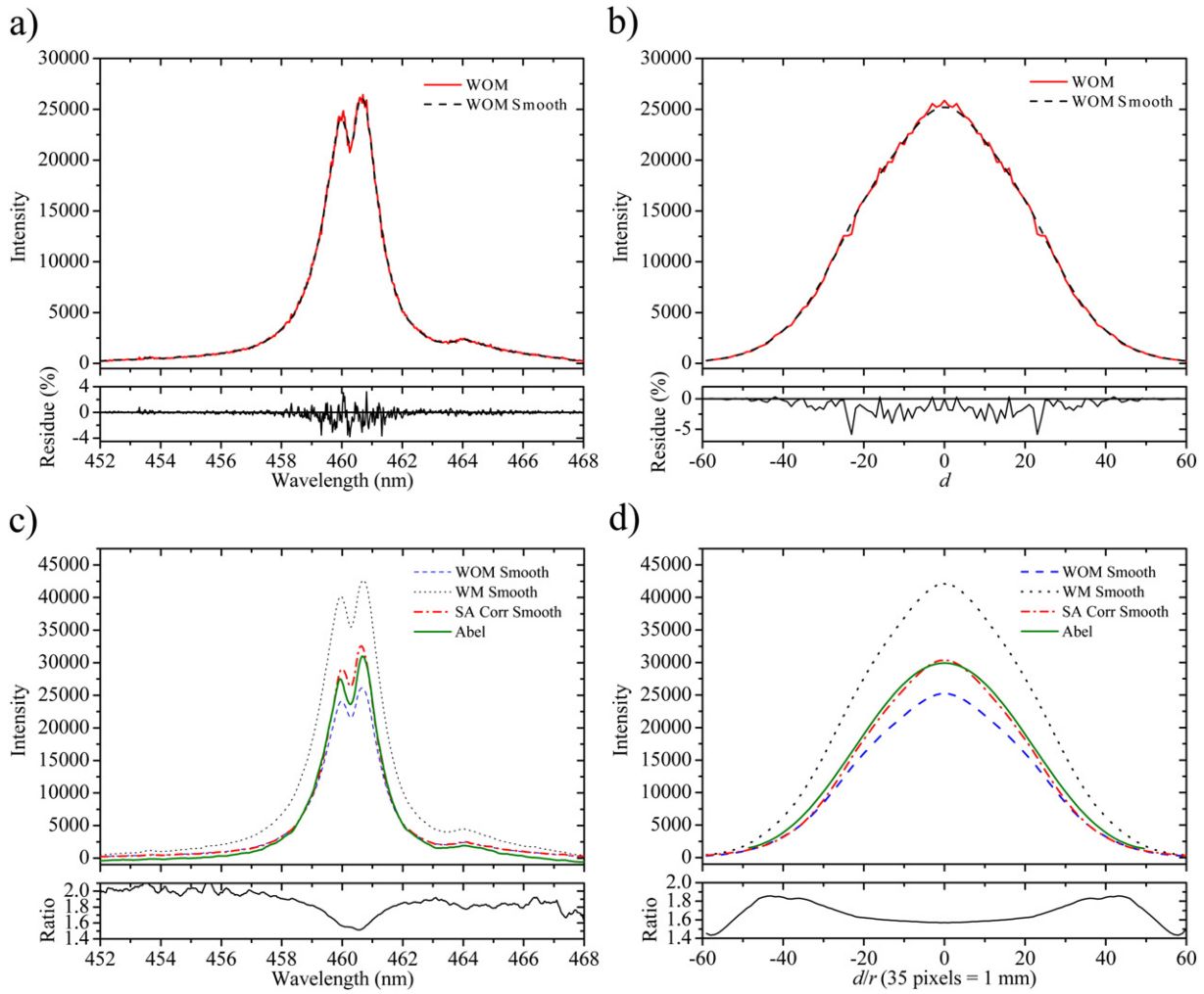


Fig. 5. The details of data processing for the Li 460.28 nm line recorded at $z = 1.5$ mm from the target surface and using delay time of $3 \mu\text{s}$. a) The spectral profile at the plasma axis recorded without back mirror (WOM) before and after smoothing. b) The lateral profile at line maximum recorded without back mirror before and after smoothing. c) The spectral profile at plasma axis recorded without back mirror (WOM) after smoothing—blue dashed line, recorded with back mirror (WM) after smoothing—black dotted line, after self absorption correction (SA Corr Smooth)—red dashed-dotted line, and after Abel inversion—green line. d) Same as c) for lateral profiles and obtained radial profile after Abel inversion—green line.

the $2p-4d$ transition, while the strongest and most important forbidden component comes from the $2p-4f$ transition. Most of studies of the Li I $2p-4d$ line with the forbidden $2p-4f$ component have been devoted to N_e plasma diagnostics and electric field strength measurements. To the best of our knowledge, the pioneering work was done by Grechikhin, see e.g. [22]. One of the important aims of his work was to derive an analytical formula for reliable N_e determination, using intensity ratio of the forbidden and allowed components (F/A) of this line. Grechikhin's study was performed at a relatively low electron density ($\sim 10^{15} \text{ cm}^{-3}$) without independent N_e diagnostics.

Besides the ratio (F/A), other parameters of complex line shape have been used for plasma N_e diagnostics. These are the separation between intensity maxima of the forbidden and allowed components (s) and a full width at half maximum of the allowed component ($FWHM_a$) [23]. These parameters, F/A , s , $FWHM_a$, were determined from generated profiles by Sassi [23] for the N_e range of $0.1-1.5 \times 10^{16} \text{ cm}^{-3}$ and compared with corresponding experimental results [22], see Section 4.2.

Further experimental and theoretical studies of lithium line shapes were related to electrolytic plasma [24,25]. As a possible explanation for disagreement between theoretical and experimental profiles, the

Table 1

Transition array, multiplet, wavelengths, lower and upper energy levels, upper level statistical weight for Li I lines used for the Boltzmann plot [31,38].

	Transition	Multiplet	Wavelength (nm)	E_l (cm^{-1})	E_k (cm^{-1})	g_k	A (10^8 s^{-1})	S
1.	$1s^2 2p-1s^2 4s$	$2p^{\circ}-^2S$	497.166	14 903.66	35 012.06	2	3.460×10^{-2}	0.42
			497.175	14 904.00	35 012.06	2	6.918×10^{-2}	0.84
2.	$1s^2 2p-1s^2 5s$	$2p^{\circ}-^2S$	427.307	14 903.66	38 299.50	2	1.59×10^{-2}	0.122
			427.313	14 904.00	38 299.50	2	3.17×10^{-2}	0.244
3.	$1s^2 2p-1s^2 5d$	$2p^{\circ}-^2D$	413.262	14 904.00	39 094.93	4	1.81×10^{-2}	0.252
			413.262	14 904.00	39 094.94	6	1.09×10^{-1}	2.27
			413.256	14 903.66	39 094.94	4	9.04×10^{-2}	1.26

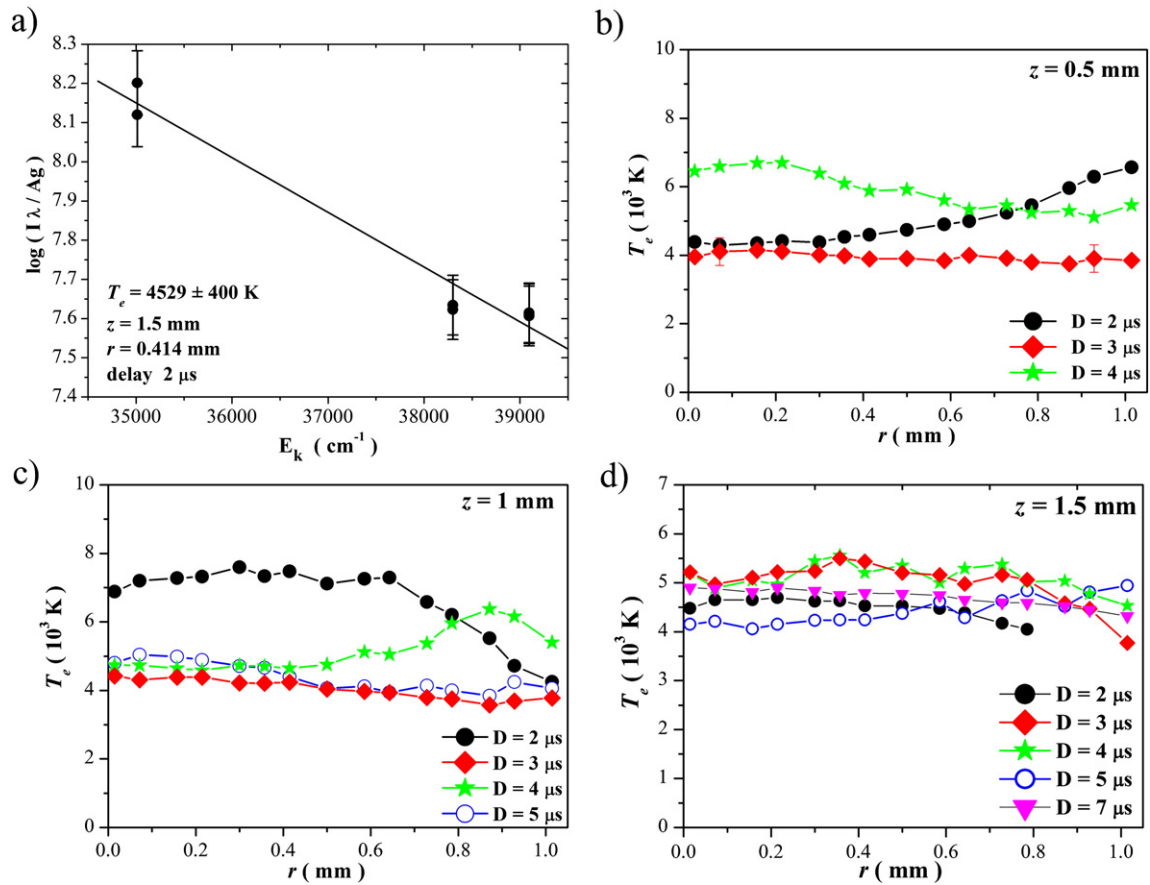


Fig. 6. a) Typical Boltzmann plot of Li I lines. Radial distributions of electron temperature at different delay times (D) at the observation distances b) $z = 0.5$ mm, c) $z = 1$ mm, d) $z = 1.5$ mm from the target surface.

authors named reabsorption of the studied lines and weakness of the quasistatic approximation assumed. The applicability range of impact approximation and dynamic role of ions to the overall profile of Li I 460.28 nm line was investigated also [25], but an independent determination of the plasma N_e and T_e is missing.

Apart from the application for N_e plasma diagnostics, Li I lines, including the 460.28 nm line, were used for electric field strength measurement induced by DC Stark effect, see e.g. [26].

From this survey it is evident that a reliable comparison between theory and experiment for the Li I 460.28 nm line is still lacking. In the first place theoretical calculations of line shapes for plasma parameters of interest have to be performed and then, for comparison the experimental line shapes recorded for known plasma N_e and T_e . In the procedure of testing theoretical calculations, an independent measurement of N_e in low-temperature plasma with a partial lithium content is a difficult task. Due to a large difference in the excitation potentials, and a low ionization potential of lithium, standard reference lines for N_e diagnostics like hydrogen Balmer lines, neutral helium lines, etc are not excited under same plasma conditions. This is another important reason for providing reliable plasma diagnostics with Li I lines, in particular, with the broad 460.28 nm line with the forbidden component. Due to the lack of other more appropriate N_e plasma diagnostic technique, we selected the isolated Li I 497.17-nm line with Stark broadening parameters calculated using two different and widely tested semi-classical approaches [10,27,28]. In addition, within this study a computer simulation method (CS) [29,30] was used to evaluate profiles of the same line, see Section 2. All three sets of theoretical data for the Li I 497.17-nm line are in good agreement (within 15%) for the studied N_e range and temperature around 5000 K. This was an argument to use this line for an independent N_e diagnostics.

The purpose of this work is to demonstrate possibility to use the Li I 460.28 nm line with the forbidden component for reliable and sensitive N_e plasma diagnostic. To achieve this goal, the computer simulation method is employed to evaluate a complex shape of this line with the forbidden component. The same computation technique is used to evaluate the line shape of the isolated and slightly asymmetric Li I 497.17 nm line. Shapes of both lines are calculated for a range of plasma electron densities. LIP is used as a light source for the experimental testing of the theoretical line shapes. The details of experimental procedure for line shape measurements in LIP are described and results of the comparison of our calculations and other theoretical results are presented and discussed. Finally, the application of the Li 460.28 nm line with the forbidden component for N_e plasma diagnostic purposes is critically evaluated and simple expressions for application of the theoretical results supplied.

2. Line-shape calculations using computer simulation method

2.1. Computational approach

For this study, shapes of the Li I 460.28-nm and 497.17-nm spectral lines were calculated using a numerical computation method described in Ref. [29], which is an implementation of computer simulation modeling of plasma-broadened line shapes [30].

In short, the perturbing fields are simulated by the Particle Field Generator (PFG), where the motion of a finite number of plasma particles (electrons and ions) is calculated assuming that classical trajectories are valid. Then, the time-dependent Schrödinger equation ($\hbar = 1$)

$$i d\Psi(t)/dt = H\Psi(t) \quad (1)$$

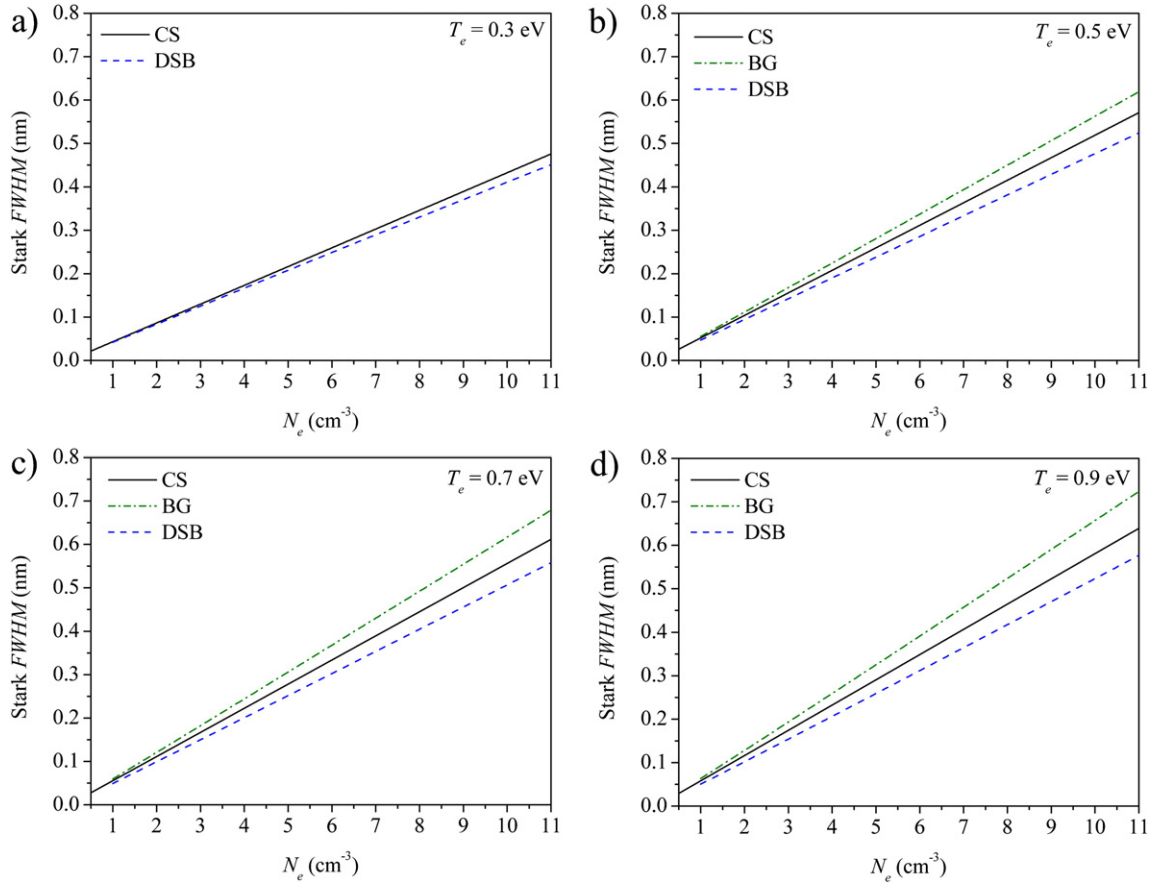


Fig. 7. Comparison of theoretical full Stark widths (electron + ion broadening) vs. N_e for different temperatures, for the Li I 497.17 nm line; blue dashed line—Dimitrijević–Sahal-Bréchet (DSB) [27,28], green dashed-dotted line—Benett and Griem (BG) [10], black line—computer simulation this work (CS); a) $T_e = 0.3$ eV (3480 K), b) $T_e = 0.5$ eV (5800 K), c) $T_e = 0.7$ eV (8120 K), and d) $T_e = 0.9$ eV (10440 K).

is numerically solved, where the Hamiltonian of the atomic system of the radiator is the sum of the unperturbed Hamiltonian H_0 and a time-dependent perturbation $V(t)$:

$$H = H_0 + V(t). \quad (2)$$

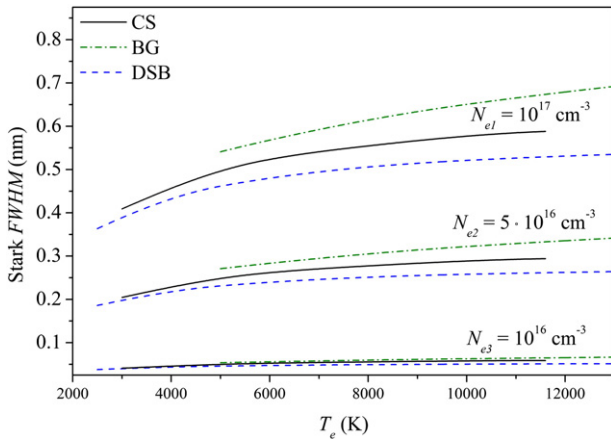


Fig. 8. Comparison of theoretical full Stark widths (electron + ion broadening) vs. T_e for three different N_e values for Li I 497.17 nm line; blue dashed line—Dimitrijević–Sahal-Bréchet (DSB) [27,28], green dashed-dotted line—Benett and Griem (BG) [10], black line—computer simulation, this work (CS).

The perturbation is due to the PFG-simulated plasma electric field and/or the macro-fields. In the interaction representation, an equivalent of Eq. (1) is

$$i d\bar{U}(t)/dt = V(t)\bar{U}(t), \quad (3)$$

where $U(t)$ is the time-development operator. The time evolution of the dipole operator $D(t)$ is then obtained:

$$\bar{D}(t) = U(t)^\dagger \bar{D}(0) U(t). \quad (4)$$

Finally, the Fourier transform of the dipole operator

$$\bar{D}(\omega) = \int_0^\infty dt \exp(-i\omega t) \bar{D}(t) \quad (5)$$

is used to calculate the line spectrum in the dipole approximation:

$$I^\lambda(\omega) \sim \frac{1}{2\pi} \sum_i \rho_i \sum_f \omega_{fi}^4 |\bar{e}_\lambda \cdot \langle \bar{D}_{fi}(\omega) \rangle|^2, \quad (6)$$

where \bar{e}_λ is the light polarization direction and each initial state i is assigned a population factor ρ_i .

2.2. Atomic data

In general, NIST atomic data [31] were used for the present calculations. However, the crucially important for the Li I 460.28-nm line shape energy difference $\Delta E_{Ad, Af} \approx 6.8 \text{ cm}^{-1}$ as inferred from the NIST database is believed to be wrong [32]. Therefore, we instead employed

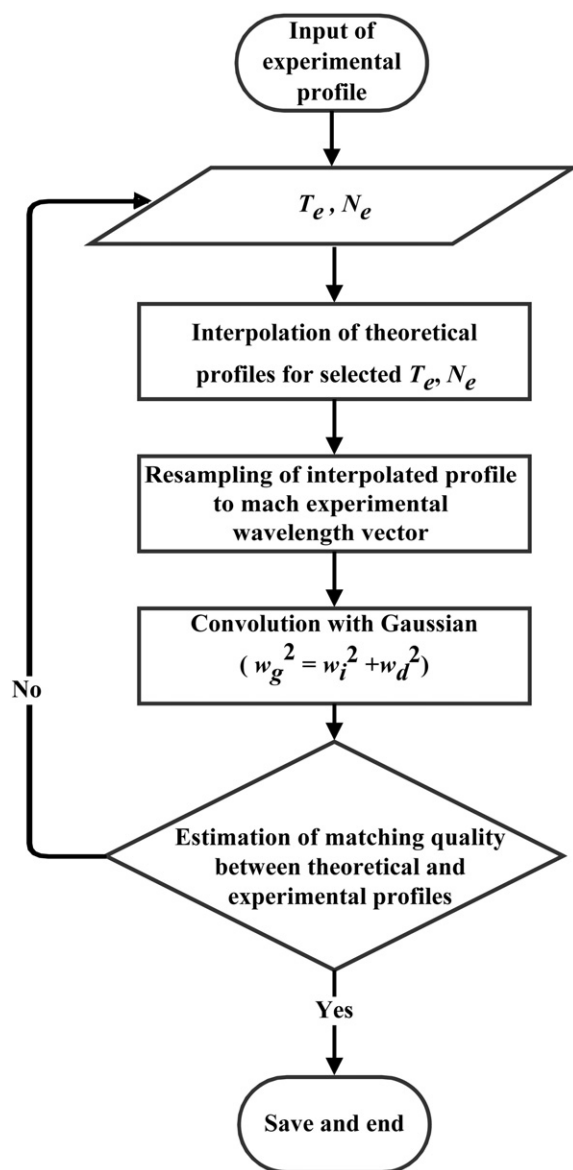


Fig. 9. Flowchart of the interpolation process and the fitting of experimental profiles. w_i represents instrumental FWHM, w_d is Doppler FWHM, and w_g is FWHM of total Gaussian.

$\Delta E_{4d,4f} \approx 5 \text{ cm}^{-1}$, derived consistently by recent theoretical studies [33, 34].

For calculations of the shape of the Li I 460.28-nm ($2p-4d$) and forbidden ($2p-4p$ and $2p-4f$) line complex, $2p$, $4s$, $4p$, $4d$, and $4f$ levels were retained in the Hamiltonian. For the Li I 497.17-nm ($2p-4s$) line broadening calculations, only $2p$, $4s$, and $4p$ were sufficient; it was verified, e.g., that addition of $2s$, $3s$, $3p$, and $3d$ levels resulted in line width increase only on the order of 1%.

2.3. Plasma modeling

The Li I 460.28-nm line at the plasma densities considered ($N_e = 10^{16} - 10^{17} \text{ cm}^{-3}$) is affected by the ion dynamics effect; therefore, in addition to the ion density, also the velocity of ions (relative to the neutral Li radiators) affects the line shape. The relative-velocity distribution is a Maxwellian with an effective (reduced) mass μ determined by the plasma composition. As it will be described in Section 3, the target pellet consisted of a mixture of Al_2O_3 , Li_2CO_3 , and MgCO_3 in a 9:4:1 proportion. Evidently, the possible values of the reduced mass might in principle vary from 3.5 (all ions are Li+) up to about 7 (heavy, possibly

molecular, ionic species). Although this effect is minor, for the Li I 460.28-nm line it may need to be included if a high accuracy is desired. As an example, in Fig. 1 we show two spectra for $T = 0.5 \text{ eV}$ (5800 K) and $N_e = 10^{17} \text{ cm}^{-3}$ calculated assuming $\mu = 3.5$ and $\mu = 5$.

On the other hand, for the 497.17-nm transition, belonging to the class of so called “isolated” lines that are largely broadened by the electron impacts [10] alone, this effect is negligible. In order to determine plasma composition, we assumed that the molecules were fully dissociated, which is a reasonable at $T \geq 0.5 \text{ eV}$. In addition, the rather long time ($> 1 \mu\text{s}$) between the application of the ablating laser and performing spectrum measurements ensures that LTE exists between atomic species and their ions. Due to different ionization potentials and statistical weights of atomic levels, the ionization degree of various species behaves differently as a function of temperature and electron density. For example, Fig. 2 shows calculated T -dependence of the plasma composition for $N_e = 10^{17} \text{ cm}^{-3}$.

The plasma particle densities derived in this way were used to simulate plasma microfields by allowing the charged plasma particles (electrons and ions) to move along classical straight-path trajectories inside a fixed spherical volume. The plasma correlation effects were accounted for by Debye screening, where the Debye length λ_s of each species s was calculated under the assumption that species heavier than s do not contribute to the screening, i.e.,

$$\lambda_s = \left[\sum_{m_j \leq m_s} \frac{4\pi n_j e^2 Z_j^2}{k_B T} \right]^{-1/2} \quad (7)$$

The number of particles was selected sufficiently large to ensure that the radius of the simulation volume exceeds the Debye length by at least three times.

3. Experimental setup

The details of our experimental setup and procedure were described in detail recently [1] and, therefore, only short description will be given for completeness. The schematic diagram of the experimental setup is given in Fig. 3a. The plasma was induced by Nd:YAG laser radiation at 1064 nm having 15 ns pulse duration and 50 mJ pulse energy. The laser beam was perpendicularly directed toward the target surface and focused by 100 mm focal length plano-convex lens. Laser-induced plasma is generated in front of a solid state surface. The target material was pellet (Al_2O_3 900 mg; Li_2CO_3 400 mg; MgCO_3 100 mg). Spectroscopic measurements were performed in air at atmospheric pressure. The image of the plasma plume was projected with 1:1 magnification (see Fig. 3), using lens with a 170 mm focal length, onto the entrance slit (10 μm width and 2.5 mm height) of the spectrometer (Shamrock sr-303i, Czerny–Turner type, focal length 303 mm) supplied with three gratings 300, 1200, and 2400 grooves/mm. A quartz lens, 50 mm diameter with a focal length of 100 mm, flat mirror and mechanical shutter were mounted behind LIP at the opposite side from the spectrometer to verify whether line self-absorption is present. The plasma radiation was recorded with the ICCD detector (Andor Technology, model DH720-18 F-63, with 1024×256 pixels, $26 \times 26 \mu\text{m}^2$ pixel size, 18 mm intensifier diameter), mounted at the exit slit plane of spectrometer. The ICCD was operated by a pulse generator (DG-535, Stanford Research Systems). The Li I lines were recorded with the 2400 grooves/mm grating. The shape of the instrumental profile is close to Gaussian with FWHM of 0.093 nm. Instrumental profiles are measured using low-pressure Hg and Ne spectral calibration lamps. The wavelength sensitivity of the spectrometer with ICCD system and all optical elements is calibrated against standard tungsten coiled-coil filament quartz halogen lamp (EG&G, model 597-1). Standard lamp was used for relative line intensity calibration. The focal plane of the laser radiation was set 1 mm below the target surface. The diameter of impact spot at the sample surface was 200 μm . The target was rotated

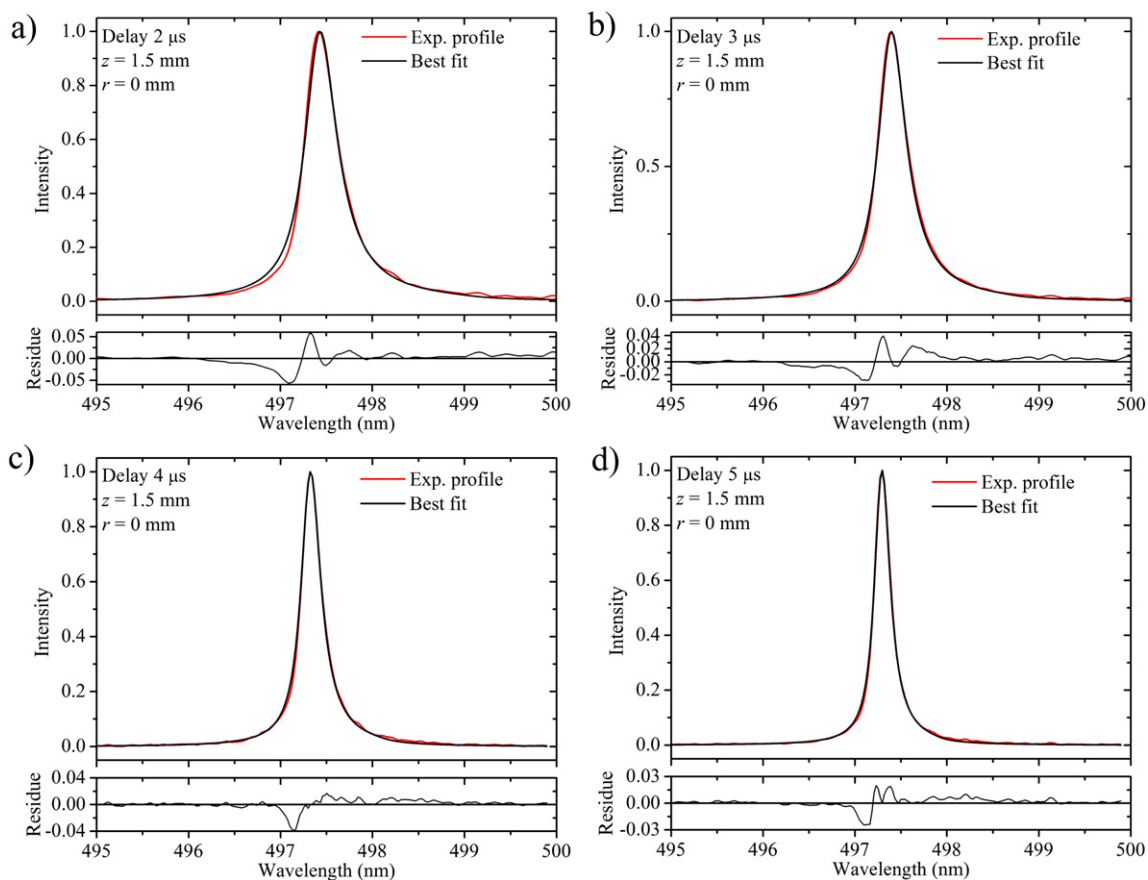


Fig. 10. Best fit examples of the Li I 497.17 nm line using CS profiles, for the delay times of a) 2 μ s, b) 3 μ s, c) 4 μ s and d) 5 μ s. All experimental profiles originate from the plasma axis at $z = 1.5$ mm from the target surface.

or translated after every 16 laser shots. Each recording is an average result of 10 accumulations, each one obtained with 16 laser shots.

The plasma plume was observed perpendicularly to the laser beam and parallel to the target surface at the distances of 0.5, 1.0 and 1.5 mm from the target surface of the pellet sample. To avoid time integration and inhomogeneity, which may affect spectral line profiles, special care was taken to select delay time and gate width. The optimum gate width of 200 ns and delay times for plasma observation of 2, 3, 4, 5, 7 μ s after laser pulse were selected. For these delay times and with 200 ns gate width, we assumed that plasma is quasi-stationary. The selected gate width and delay times were appropriate also to avoid strong plasma continuum emission and to enhance signal-to-background ratio, see [1] for more details.

3.1. Data processing

The recorded spectral image represents spectral radiance emitted by the observed LIP layer as a function of the lateral position and wavelength. The radiation detected by each pixel of the ICCD matrix corresponds to an integrated intensity of the plasma emission along the line-of-sight across the radius of the plasma plume. An example of spectrum is given in Fig. 4a. The details of the experimental data processing were also described recently [1] and only a short description will be given. The procedure consists of several steps which are illustrated in Figs. 4 and 5. At the first step, spectral images are imported along with the correction factor (the apparatus function). After intensity and wavelength corrections, the images (1st one recorded without the back mirror and 2nd one recorded with the back mirror) are cropped along the wavelength and lateral axes and symmetrized (Fig. 4a and b). Then images are smoothed using Savitzky–Golay filter (Figs. 4c,d, 5a,b). In the next step self-absorption correction procedure is performed

(Figs. 4e and 5c,d). The details of self-absorption correction and conditions of their applicability are given in [1,2]. After checking that a line is optically thin (or that it can be corrected to optically thin case), an Abel inversion procedure is performed (Figs. 4f and 5c,d).

4. Results and discussion

4.1. Plasma diagnostics

4.1.1. Electron temperature

For the electron temperature (T_e) determination Boltzmann plot (BP) technique was employed, using relative intensities of Li I lines given in Table 1. Prior to calculation of T_e , the issue of BP technique applicability under LIP conditions was addressed. The discussion about BP technique and partial local thermal equilibrium (pLTE) existence in LIP plasma is given in recent publications [1,2]. The upper levels of transitions used for T_e determination have to be in pLTE in order to have valid T_e diagnostic by the Boltzmann plot technique. Applying the same procedure as in [1,2] determined critical quantum number at pLTE limit is 2, calculated using Eq. (7.77) from [35] for lowest N_e and T_e . This means that all Li I lines with the upper level principal quantum number 3 (ground state + next level) or higher can be used for the T_e determination using the BP technique. From Table 1 one can see that all three Li I lines fulfill pLTE condition. On the other hand, the so called McWhirter criterion, commonly used for estimation of LTE presence in LIP, gives value of $N_e = 6.38 \times 10^{15} \text{ cm}^{-3}$ (Eq. (12) in [36], see also [37]) for critical electron density above which LTE is established. According to this criterion, all levels of Li I could be used under given experimental conditions. These two considerably different results indicate that, generally speaking, criteria for LTE assessment are not well defined in literature, see also [36].

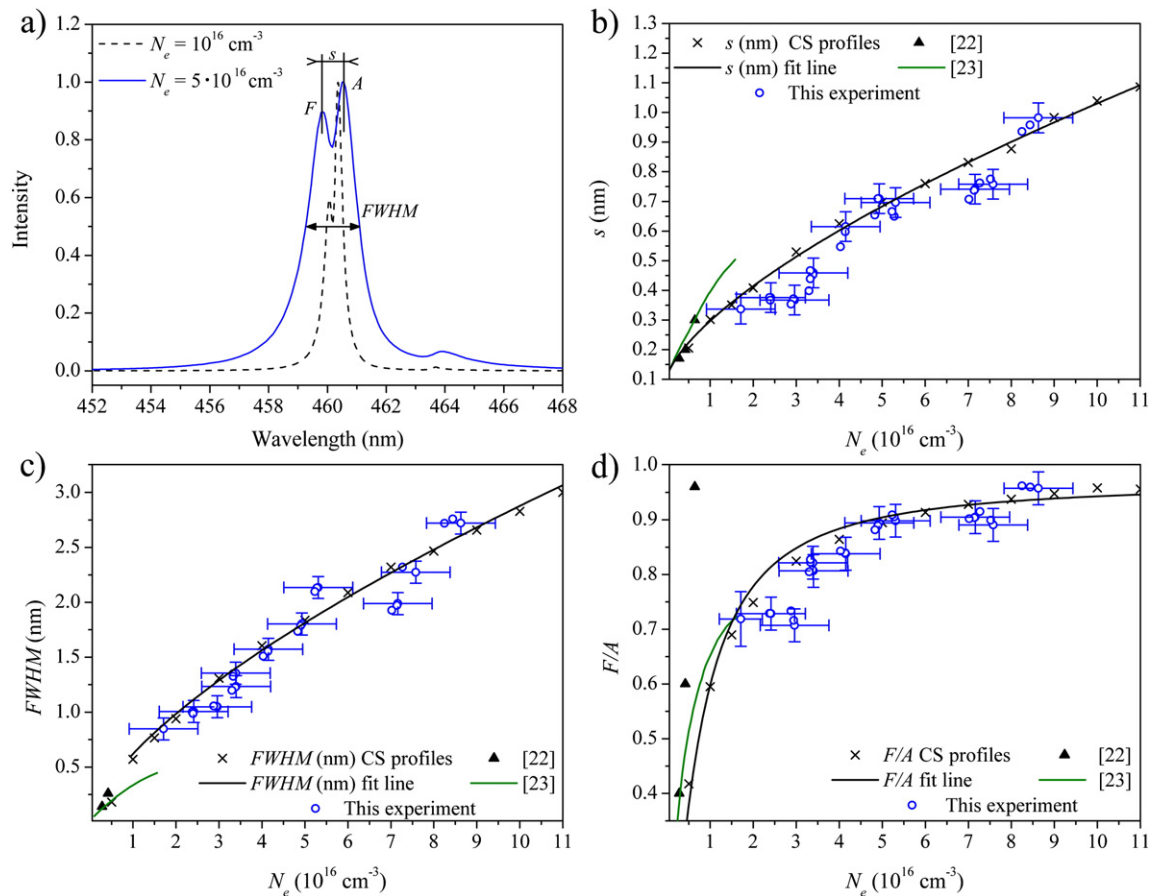


Fig. 11. a) The illustration of spectral line parameters that describe the profile of Li I 460.28 nm line with forbidden component, s —separation between allowed (A) and blue forbidden (F) component, intensity ratio F/A , $FWHM$ —full width at half maximum of the total profile (allowed + forbidden), b), c) and d) comparison between theoretical s , $FWHM$, F/A dependence and experimental results. For experimental results N_e is determined from best fits of Li I 497.17 nm experimental profiles lines using CS line shapes. In Fig. 11c. CS fit line describes Stark $FWHM$ (allowed + forbidden), while green line from [23] describes $FWHM$ of allowed component only. The reason for this difference: the calculations [23] were performed for low N_e when the peak intensity of forbidden line is smaller than the halfwidth intensity of allowed line.

A typical Boltzmann plot with Li I lines is shown in Fig. 6a, while radial distributions of T_e are given in Fig. 6b,c,d. The estimated uncertainty of T_e measurements is in the range of 8% to 12% depending upon delay time i.e. intensities of Li I lines.

4.1.2. Electron density from Li I 497.17 nm line

The H_{α} Balmer line, frequently used for the N_e plasma diagnostics, was very weak or not visible at the long delay times ($>2.5 \mu\text{s}$) which were of interest for the study of Li I lines. At these late times Li I lines of interest are present and clearly visible in terms of good signal to noise and signal to background ratios. Furthermore, for early delay times ($<2 \mu\text{s}$), Li I 460.28 nm line was very broad interfering with other neighboring lines like, e.g., the Al II 466.30 nm line. These broad and interfering line profiles were not used for the line shape analysis in this study. As discussed earlier, for an independent method for N_e plasma diagnostics, the Li I 497.17 nm line was chosen. For this line two sets of semiclassical calculations by Benett and Griem (BG), see Appendix IV in [10], and Dimitrijevic and Sahal-Bréchet [27,28] were already available but the difference between data was not negligible. In order to determine which set of data to use for N_e plasma diagnostics we performed calculation of the Stark widths for the same line using the CS method (see Section 2) and all results are presented in Fig. 7.

Before discussing mutual comparison of theoretical results in Fig. 7, let us point out that both data sets BG [10] and DSB [28] were used to infer experimental Stark profiles of Mg I lines [1]. Same procedure described in [1] is applied here with experimental Li I line profiles for N_e plasma diagnostics whenever using Stark broadening data BG [10] and DSB [27,28]. Here, it should be mentioned that the DSB data set

[27,28] lists only the electron impact widths, so the ion broadening parameter A was taken from [10] to infer total Stark widths (see Fig. 7).

The comparison of the theoretical data in Figs. 7 and 8 shows that both sets of already available Stark-broadening Li I data [10,27,28] are in a reasonable agreement with the CS results. In this study CS Stark profiles of the Li I 497.17 nm line were used for an independent plasma N_e diagnostics of LIP since line shape evaluation is performed for entire asymmetric line profile for all studied plasma conditions. In addition to this advantage, the same code as for the Li I 460.28 nm line is used, so if there is certain minor inadequacy of the model, it is present for both lines and hence it should cancel out.

The set of CS theoretical Stark profiles of the Li I 497.17 nm line calculated for an N_e range of $(0.5 - 11) \times 10^{16} \text{ cm}^{-3}$ and $T_e = 0.3, 0.5, 0.7, 0.9 \text{ eV}$ (3480, 5800, 8120, 10440 K) were used (see Figs. 7 and 8) to determine LIP radial distributions of N_e . For $N_e < 5 \times 10^{16} \text{ cm}^{-3}$, the experimental widths were determined by fitting measured profile with asymmetric profile function $j_{A,R}$ [1,10] convoluted with Gaussian, which includes instrumental and Doppler broadening. Then full Stark width is used to determine N_e from data in Fig. 7 (solid black line). For higher electron densities ($>5 \times 10^{16} \text{ cm}^{-3}$) whole experimental profile is fitted with theoretical CS profile. To obtain intermediate values from the CS data set, an interpolation procedure is applied. The fitting procedure with interpolated profiles is shown as a flowchart in Fig. 9. By varying N_e , the best fit of experimental data is achieved and N_e is inferred. Typical experimental profiles fits are shown in Fig. 10. Criteria for a satisfactory matching between the experimental and interpolated theoretical profiles were set for the residue to be less than ± 0.05 and for the correlation coefficient to exceed 0.98.

Table 2

Comparison of experimental and theoretical data for different N_e and T_e . Values of N_e are deduced from the Li I 497.17 nm line using the CS data set. Spectral profile parameters of Li I 460.28 nm line s , F/A , and w are illustrated in Fig. 11a. Here, w represents full width at the half maximum (FWHM). All theoretical data are calculated for $T_e = 5800$ K.

N_e (10^{16} cm $^{-3}$)	T_e (K)	s_m (nm)	s_m/s_{th}	$(F/A)_m$	$(F/A)_m/(F/A)_{th}$	w_m (nm)	w_m/w_{th}
8.63	4470	0.98	1.03	0.96	1.01	2.72	1.03
8.44	4650	0.96	1.02	0.96	1.02	2.76	1.06
8.25	4620	0.93	1.00	0.96	1.02	2.72	1.06
7.58	6880	0.76	0.85	0.89	0.95	2.27	0.93
7.52	7270	0.77	0.88	0.90	0.96	2.34	0.96
7.27	7600	0.76	0.88	0.91	0.98	2.32	0.97
7.16	5210	0.74	0.86	0.90	0.97	1.99	0.84
7.14	5100	0.74	0.86	0.90	0.97	1.97	0.83
7.02	5240	0.71	0.83	0.90	0.97	1.93	0.82
5.31	4390	0.70	0.97	0.90	1.00	2.13	1.10
5.28	4350	0.65	0.91	0.90	1.01	2.13	1.11
5.23	4380	0.66	0.94	0.91	1.01	2.10	1.10
4.93	5210	0.71	1.04	0.89	1.00	1.80	0.98
4.90	5050	0.71	1.04	0.89	1.00	1.79	0.98
4.83	5450	0.65	0.97	0.88	0.99	1.73	0.96
4.15	4150	0.61	1.00	0.84	0.96	1.57	0.98
4.14	4060	0.60	0.97	0.84	0.96	1.55	0.97
4.03	4230	0.55	0.90	0.84	0.97	1.51	0.96
3.40	4900	0.46	0.84	0.81	0.96	1.23	0.89
3.38	4800	0.46	0.85	0.81	0.96	1.23	0.89
3.30	4830	0.40	0.74	0.80	0.96	1.20	0.89
3.36	3960	0.45	0.84	0.82	0.98	1.35	0.99
3.33	4150	0.47	0.87	0.82	0.98	1.35	0.99
3.33	4010	0.44	0.81	0.83	0.98	1.33	0.99
2.96	4740	0.37	0.73	0.71	0.86	1.05	0.85
2.94	4650	0.37	0.74	0.72	0.87	1.05	0.86
2.88	4730	0.35	0.72	0.73	0.90	1.06	0.87
2.41	4800	0.38	0.84	0.73	0.93	1.01	0.96
2.38	4990	0.38	0.85	0.73	0.93	1.00	0.96
2.40	4710	0.37	0.82	0.73	0.93	0.99	0.94
1.71	6450	0.34	0.90	0.72	1.00	0.85	1.06
1.71	6690	0.34	0.91	0.72	1.00	0.84	1.06
1.71	6390	0.34	0.90	0.71	0.99	0.83	1.05

The estimated uncertainty of the reported N_e values from the Li I 497.17 nm line is based on a detailed comparison of the BG semiclassical results [10] with various experiments, see Appendix A in Ref. [39]. It was estimated for several multiplets of light elements (He I, C I and N I) that the semiclassical data [10] may be used for N_e diagnostics with an uncertainty in the range of 12% to 17%. For all calculated and tested neutral atom lines from He through Ca the average uncertainty value is 20% [39]. Since we are dealing here with lithium, which is a light element with a simple atomic energy structure, and having in mind comparison in Fig. 7 with two other well tested calculations, the estimated uncertainty of reported N_e results is in the range of 10% and 15% depending upon quality of experimental line profiles.

4.2. Stark broadening of Li I 460.28 nm line

Theoretical CS profiles of the Li I 460.28 nm line with the forbidden components were calculated for same N_e mesh as the Li I 497.17 nm

Table 3

Average value of experimental to theoretical ratio for Li 460.28 nm line spectral profile parameters. N_e ranges were determined from the Stark widths of the Li I 497.17 nm line using the BG [10], DSB [27,28], and CS calculations—the first column in the table. Temperature range is $T_e = (3960 - 7270)$ K.

	N_e (10^{16} cm $^{-3}$)	(s_m/s_{th}) average	$((F/A)_m/(F/A)_{th})$ average	(w_m/w_{th}) average
N_e range from Li 497.17 nm line using BG data set	1.60–7.80	0.96	0.98	1.03
N_e range from Li 497.17 nm line using DSB data set	2.10–8.85	0.85	0.95	0.90
N_e range from Li 497.17 nm line using CS data set	1.71–8.63	0.89	0.97	0.97

line but for $T_e = 5800$ K only. From these CS profiles line parameters s , $FWHM$ and F/A were determined (black crosses in Fig. 11) and then theoretical dependences of these parameters versus N_e deduced (see Fig. 11, black lines). Here, s is the separation between the allowed (A) and the short-wavelength, “blue”, forbidden (F) component, $FWHM$ is a full width at half maximum of the total profile (the allowed + forbidden components), and F/A is the peak intensity ratio of the forbidden to allowed component. Besides theoretical dependences of line parameters, the experimental values are shown in Fig. 11 as data points for N_e values inferred from the CS data set for the Li I 497.17 nm line. For the sake of completeness, available data from [22,23] were also included in Fig. 11.

Experimentally determined Li I 460.28 nm line parameters: s , $FWHM$ and F/A and their experimental to theoretical ratios are also given in Table 2.

For the sake of comparison of plasma N_e results derived from the CS Li I 497.17 nm line profiles (see Table 2) with N_e from the BG [10] and DSB [27,28] data, N_e range derived from all three data sets are presented in Table 3. Average experimental to theoretical ratios of line parameters s , $FWHM$ and F/A of the Li I 460.28 nm line are also given in Table 3.

The comparison of the theoretical and experimental Li I 460.28 nm line profiles is presented in Fig. 12. The theoretical CS profiles are interpolated in a similar way as the Li I 497.17 nm line for N_e values inferred from CS Li I 497.17 nm line profiles. The agreement between theoretical and experimental profiles is checked for several N_e values and differences are presented in the form of residue graphs in Fig. 12. These differences are in the range -0.1 to 0.1 , when both profiles are normalized to peak intensity.

The comparison of the experimental and theoretical profiles in Fig. 12 shows a reasonable agreement, and therefore, we conclude that the CS profiles correctly describe the overall profile of the Li I 460.28 nm line with the forbidden component at the “blue” line wing. Therefore, to simplify further use of the theoretical data for plasma N_e diagnostics we derive best fit formulas that describe dependence of s , $FWHM$ and F/A on N_e .

$$s \text{ (nm)} = \sqrt{0.1059^2 + 0.036 \cdot \left(\frac{N_e}{10^{16} \text{ cm}^{-3}}\right)^{2/3} + 0.041 \cdot \left(\frac{N_e}{10^{16} \text{ cm}^{-3}}\right)^{4/3}} \quad (8)$$

$$FWHM \text{ (nm)} = 0.62 \cdot \left(\frac{N_e}{10^{16} \text{ cm}^{-3}}\right)^{2/3} \quad (9)$$

$$F/A = \frac{0.97 \cdot \left(\frac{N_e}{10^{16} \text{ cm}^{-3}}\right)^{4/3}}{0.62 + \left(\frac{N_e}{10^{16} \text{ cm}^{-3}}\right)^{4/3}} \quad (10)$$

The expressions (8) and (10) may be used in the N_e range of $0.5 - 11 \times 10^{16}$ cm $^{-3}$ and $T_e = 5800$ K, while the expression (9) is for the range of $1 - 11 \times 10^{16}$ cm $^{-3}$ and $T_e = 5800$ K since it describes total $FWHM$ (allowed + forbidden). For N_e below $\sim 10^{16}$ cm $^{-3}$, F/A ratio falls below 0.5 so only $FWHM$ of allowed component can be determined. It should be pointed out that preliminary test of the Li I 460.28 nm line shape shows a weak dependence on T_e ; therefore, (8–10) may be used with confidence for the temperature range of (4000 – 7000) K.

5. Summary and conclusions

We reported results of theoretical and experimental study of the Li I 460.28 nm line with the forbidden component in low temperature plasma. To perform this study a computer simulation method was used to calculate the overall shape of this line in the electron density range of $0.5 - 11.0 \times 10^{16}$ cm $^{-3}$ and electron temperature of 0.5 eV (5800 K). The same computation technique was used for line shape calculations of the isolated Li I 497.17 nm line in the same electron density range and for electron temperatures 0.3, 0.5, 0.7, and 0.9 eV

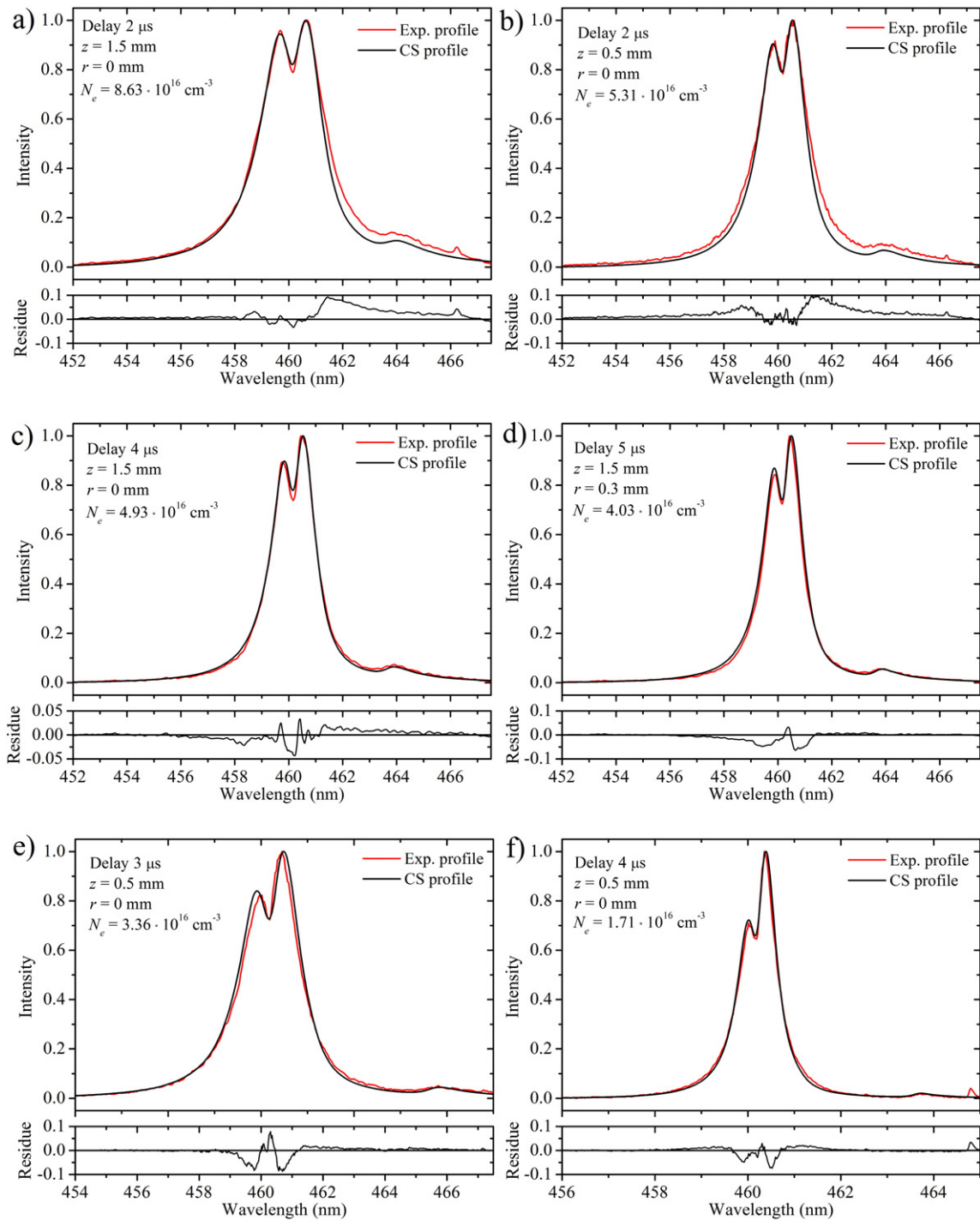


Fig. 12. Comparison of theoretical and experimental profiles for the Li I 460.28 nm line. Theoretical CS profiles are generated for N_e values inferred from best fits of the experimental Li I 497.17 nm profiles using the CS data set.

(3480, 5800, 8120, 10440 K). These results were compared with two other sets of semiclassical calculations used for plasma electron density diagnostics.

The shapes of the lithium lines studied were recorded from laser induced plasma, which was used as a light source for this experiment. The plasma was induced with a pulsed Nd:YAG laser at 1.06 μm irradiating pellet target containing a lithium compound. The experimental details and data handling procedure were described. Plasma parameters were determined at the time of line shape studies. The electron temperature was determined from relative intensities of several Li I lines by applying the Boltzmann plot technique. The electron density was inferred from

the shape of the Li I 497.17 nm line using all three sets of theoretical calculations. However, the test of Li I 460.28 nm line with the forbidden component was carried out on the basis of electron density derived from the computer simulation results for the Li I 497.17 nm line. These results were selected for two reasons: (i) they provide whole asymmetric line profile and (ii) the same code as for the Li I 460.28 nm line is used for modeling. The estimated uncertainty of plasma electron density measurements is in the range of 10–15%.

Theoretical line shape parameters of the Li I 460.28 nm line with the forbidden component were tested by comparison with measured values (see Fig. 11) while the experimental N_e values were determined

by using the Li I 497.17 nm line shapes. The comparison of whole shape of theoretical and experimental profiles was presented in Fig. 12. The theoretical profiles in this figure were generated for the experimental electron densities, obtained from the Li I 497.17 nm line, as shown in Fig. 11.

On the basis of comparison theory versus experiment we concluded that theoretical data for Li I 460.28 nm line with the forbidden component may be used with confidence for electron density plasma diagnostics at the temperature of about 0.5 eV (5800 K) with an estimated uncertainty in the range of 10–15%. In order to avoid detailed analysis of the Li I 460.28 nm line profiles, the best fits of line parameters s , F/A , and $FWHM$ are described by formulas (8–10). By measuring the line shape parameters one can not only determine electron density, but also estimate whether the lines are self-absorbed.

Acknowledgments

This work is supported by the Ministry of Education, Science and Technological Development of the Republic Serbia under Project no. 171014. The work of E. Stambulchik was supported in part by the Israel Science Foundation grant no. 711618 and Cornell Center of Excellence for the Study of Pulsed-Power-Driven High Energy Density Plasma Studies, grant no. 703142.

References

- [1] M. Cvejić, M.R. Gavrilović, S. Jovičević, N. Konjević, Stark broadening of Mg I and Mg II spectral lines and Debye shielding effect in laser induced plasma, *Spectrochim. Acta Part B* 85 (2013) 20–33.
- [2] M. Cirisan, M. Cvejić, M.R. Gavrilović, S. Jovičević, N. Konjević, J. Hermann, Stark broadening measurements of Al II lines in laser-induced plasma, *J. Quant. Spectrosc. Radiat. Transf.* 133 (2014) 652–662.
- [3] A.M. El Sherbini, A.-N. Aboufotouh, F. Rashid, S.H. Allam, A.M. Al-Kaoud, A. El Dakroui, T.M. El Sherbini, Spectroscopic measurement of Stark broadening parameter of the 636.2 nm Zn I-line, *Nat. Sci.* 5 (2013) 501–507.
- [4] E. Axente, J. Hermann, G. Socol, L. Mercadier, S.A. Beldjilali, M. Cirisan, C.R. Luculescu, C. Ristoscu, I.N. Mihailescu, V. Craciuna, Accurate analysis of indium–zinc oxide thin films via laser-induced breakdown spectroscopy based on plasma modeling, *J. Anal. At. Spectrom.* 29 (2014) 553–564.
- [5] C. Aragón, J.A. Aguilera, J. Manrique, Measurement of Stark broadening parameters of Fe II and Ni II spectral lines by laser induced breakdown spectroscopy using fused glass samples, *J. Quant. Spectrosc. Radiat. Transf.* 134 (2014) 39–45.
- [6] J.A. Aguilera, J. Manrique, C. Aragón, Stark width measurements of Fe II lines with wavelengths in the range 230–260 nm, *J. Phys. B: At. Mol. Opt. Phys.* 44 (2011) 245701 (6 pp.).
- [7] M. Skočić, M. Burger, Z. Nikolić, S. Bukvić, S. Djeniže, Stark broadening in the laser-induced Cu I and Cu II spectra, *J. Phys. B: At. Mol. Opt. Phys.* 46 (2013) 185701 (6 pp.).
- [8] M. Burger, M. Skočić, Z. Nikolić, S. Bukvić, S. Djeniže, Broadening of the resonance Cu I lines in the laser-induced copper spectrum, *J. Quant. Spectrosc. Radiat. Transf.* 133 (2014) 589–595.
- [9] N. Konjević, J.R. Roberts, A critical review of the Stark widths and shifts of spectral lines from non-hydrogenic atoms, *J. Phys. Chem. Ref. Data* 5 (1976) 209–257.
- [10] H.R. Griem, *Spectral Line Broadening by Plasmas*, Academic Press, New York, 1974.
- [11] G. Bekefi, C. Deutsch, B. Yaakobi, *Principles of Laser Plasmas*, John Wiley & Sons, New York, 1976.
- [12] M. Ivković, M.A. Gonzalez, S. Jovičević, M.A. Gigosos, N. Konjević, A simple line shape technique for electron number density diagnostics of helium and helium-seeded plasmas, *Spectrochim. Acta Part B* 65 (2010) 234–240.
- [13] M.A. Gonzalez, M. Ivković, M.A. Gigosos, S. Jovičević, N. Lara, N. Konjević, Plasma diagnostics using the He 447.1 nm line at high and low densities, *J. Phys. D Appl. Phys.* 44 (2011) 194010 (7 pp.).
- [14] M. Ivković, M.A. Gonzalez, N. Lara, M.A. Gigosos, N. Konjević, Stark broadening of the He I 492.2 nm line with forbidden components, in dense low temperature plasma, *J. Quant. Spectrosc. Radiat. Transf.* 127 (2013) 82–89.
- [15] X. Bai, Q. Ma, M. Perrier, V. Motto-Ros, D. Sabourdy, L. Nguuyen, A. Jalocho, J. Yu, Experimental study of laser-induced plasma: influence of laser fluence and pulse duration, *Spectrochim. Acta. Part. B* 87 (2013) 27–35.
- [16] T. McCormack, G. O'Sullivan, Spatially resolved spectra of resonantly pumped laser produced plasmas of lithium, *Rev. Sci. Instrum.* 70 (1999) 2674–2680.
- [17] M.E. Sherill, R.C. Mancini, J.E. Bailey, A. Filuk, B. Clark, P. Lake, J. Abdallah, Spectroscopic diagnostics of low temperature laser ablated LiAg plasma plume, *Rev. Sci. Instrum.* 72 (2001) 957–960.
- [18] I. Labazan, S. Milošević, Determination of electron density in a laser-induced lithium plume using cavity ring-down spectroscopy, *J. Phys. D Appl. Phys.* 37 (2004) 2975–2980.
- [19] M.A. Baig, Aisha Qamar, M.A. Fareed, M. Anwar-ul-Haq, Raheel Ali, Spatial diagnostics of the laser induced lithium fluoride plasma, *Phys. Plasmas* 19 (2012) 063304 (5 pp.).
- [20] R.W. Coons, S.S. Harial, M. Polek, A. Hassanein, Spatial and temporal variations of electron temperatures and densities from EUV-emitting lithium plasmas, *Anal. Bioanal. Chem.* 400 (2011) 3239–3246.
- [21] N. Konjević, M.S. Dimitrijević, W.L. Wiese, Experimental Stark widths and shifts for spectral lines of neutral atoms (a critical review of selected data for the period 1976 to 1982), *J. Phys. Chem. Ref. Data* 13 (1984) 619–647.
- [22] L.I. Grechikhin, E.S. Tyumina, Forbidden lines of sodium and lithium in the flame of a dc arc, *High Temp. (USSR)* 1 (1963) 358.
- [23] M. Sassi, Determination de la densité électronique d'un plasma ionisé à partir de la distance entre les pics de la raie 'permise' LiI (22P–42D) (ou CsI (5D3/2–6 F)) et de la raie 'interdite' LiI (22P–42 F) (ou CsI (5D3/2–6G)), *J. Quant. Spectrosc. Radiat. Transf.* 12 (1972) 75–96.
- [24] T. Biaz, J.C. Valognes, P. Mergault, Etude spectroscopique de l'effet d'anode, *J. Quant. Spectrosc. Radiat. Transf.* 14 (1974) 27–34.
- [25] J.P. Bardet, J.C. Valognes, Application du formalisme exponentiel de Magnus au calcul du profil de la raie semi-dégénérée (4f 4d 4p – 2p) du lithium émise par un plasma électrolytique (Effet d'anode), tenant compte de l'Effet dynamique des ions, *J. Phys.* 47 (1986) 1203–1220.
- [26] Б.А. Князев, С.В. Лебедев, П.И. Мельников, Активная штарковская спектроскопия атомного пучка как метод измерения электрических полей, *J. Tech. Phys.* 61 (1991) 6–18.
- [27] M.S. Dimitrijević, S. Sahal-Bréchet, Broadening of Li(I) lines by collisions with charged particles, *Bull. Obs. Astron. Belgrade* 143 (1991) 29–48.
- [28] S. Sahal-Bréchet, M.S. Dimitrijević, N. Morecbau, Stark-B database, Observatory of Paris, IERMA and Astronomical Observatory of Belgrade, (online). Available <http://stark-b.obspm.fr> June 18 2013.
- [29] E. Stambulchik, Y. Maron, A study of ion-dynamics and correlation effects for spectral line broadening in plasma: K-shell lines, *J. Quant. Spectrosc. Radiat. Transf.* 99 (2006) 730–749.
- [30] E. Stambulchik, Y. Maron, Plasma line broadening and computer simulations: a mini-review, *High Energy Dent. Phys.* 6 (2010) 9–14.
- [31] A. Kramida, Yu. Ralchenko, J. Reader, NIST ASD Team, NIST Atomic Spectra Database (version 5.1), <http://physics.nist.gov/asd> 2013 (Accessed January, 2014).
- [32] K. Tsigutkin, E. Stambulchik, Y. Maron, A. Tauschwitz, Determination of the Li I 4d–4f energy separation using active spectroscopy, *Phys. Scr.* 71 (2005) 502–506.
- [33] M.S. Safronova, C.F. Fischer, Yu. Ralchenko, Relativistic all-order and multiconfiguration Hartree–Fock calculations of the 4d–4f energy separation in Li I, *Phys. Rev. A* 76 (2007) 054502.
- [34] W.R. Johnson, U.I. Safronova, A. Derevianko, M.S. Safronova, Relativistic many-body calculation of energies, lifetimes, hyperfine constants, and polarizabilities in ${}^7\text{Li}$, *Phys. Rev. A* 77 (2008) 022510.
- [35] H.R. Griem, *Principles of Plasma Spectroscopy*, Cambridge University Press, 1997.
- [36] G. Cristoforetti, A. De Giacomo, M. Dell'Aglio, S. Legnaioli, E. Tognoni, V. Palleschi, N. Omenetto, Local thermodynamic equilibrium in laser-induced breakdown spectroscopy: beyond the McWhirter criterion, *Spectrochim. Acta Part B* 65 (2010) 86–95.
- [37] R.W.P. McWhirter, in: R.H. Huddlestone, S.L. Leonard (Eds.), *Plasma Diagnostic Techniques*, Academic Press, New York, 1965, pp. 201–264, (Chapter 5).
- [38] W.L. Wiese, J.R. Fuhr, Accurate atomic transition probabilities for hydrogen, helium, and lithium, *J. Phys. Chem. Ref. Data* 38 (2009) 565–719.
- [39] N. Konjević, Plasma broadening and shifting of non-hydrogenic spectral lines: present status and applications, *Phys. Rep.* 316 (1999) 339–401.